Non-Linear Landau Damping of Plasma Waves with Orbital Angular Momentum

D. R. Blackman,[1,2] R. Nuter,[2] Ph. Korneev,[3,4] and V.T. Tikhonchuk[2,5]

[1]*Mechanical and Aerospace Engineering, University of California San Diego, 9500 Gilman Drive, La Jolla, CA 92093-0411, USA*

[2]*CELIA, University of Bordeaux, CNRS, CEA, 33405 Talence, France*

[3]*National Research Nuclear University "MEPhI" (Moscow Engineering Physics Institute), Moscow, 115409 Russia*

[4]*P. N. Lebedev Physics Institute, Russian Academy of Sciences, 119991 Moscow, Russia*

[5]*ELI-Beamlines, Institute of Physics, Czech Academy of Sciences, 25241 Dolní Břežany, Czech Republic*

Abstract

We present, using three-dimensional Particle-In-Cell simulations, an observation that orbital angular momentum is transferred to resonant electrons proportionally to longitudinal momentum when Laguerre-Gaussian plasma waves are subject to Landau damping. A higher azimuthal mode number leads to a larger net orbital angular momentum in particles travelling close to the phase velocity of the plasma wave, implying a population of electrons that are orbiting the same centre of rotation as the plasma wave. This observation has implications on magnetic field excitation as a result of the formation and damping of OAM plasma waves. The energy distributions of electrons in damping Laguerre-Gaussian plasma waves are significantly changed as a function of azimuthal mode number. This leads to larger numbers of lower energy particles tending towards a mono-energetic bunching.

I. INTRODUCTION

Electromagnetic waves carrying orbital angular momentum (OAM), described as Laguerre-Gaussian solutions to the paraxial equation in cylindrical geometry [1], have a variety of applications in optics with low-intensity beams for compact storing of information, nano-scale imaging and manipulation [2]. More recently applications at higher intensities are showing the potential of OAM light in particle focusing and acceleration, and generation of strong plasma waves, and quasi-static magnetic fields [3–6].

A proper description of the propagation of electromagnetic waves with OAM through a plasma requires the understanding of excitation and evolution of electrostatic waves (plasmons) carrying OAM [7]. In addition to this, these OAM plasmons may have applications of their own, as several studies [8, 9] show, for the generation of complex quasi-static magnetic fields.

The description of OAM plasmons damping requires the kinetic framework. However, the Laguerre-Gaussian (LG) functions are not the eigenfunctions of the electron kinetic equation. For this reason, a simplified consideration [10] leads to an inaccurate expression of the dispersion, and thus the phase velocity, and damping of these waves even in the linear regime. A more consistent approach using the expansion on the paraxial parameter – the ratio of the plasma wavelength $2\pi/k$ to the radial width of the wave packet w_b (or more conveniently written as $1/kw_b$) - leads to dispersion and damping coefficients being shown to be strongly mode dependent in certain regimes[8].

For an electron, with a sufficiently small initial velocity v, travelling through a low amplitude plasma wave, the electric field of an OAM plasma wave reversibly transfers linear momentum and orbital momentum to the particle during one half cycle and then back in the second. When the plasma wave is damped this symmetry is broken and momentum, both linear, and possibly orbital angular momentum, can be transferred. Calculations have been performed previously to find the proportion of angular momentum transferred from the electrostatic wave to individual particles [11]. Our aim is to study the irreversible transfer occurring via Landau damping in the non-linear regime where particle trapping can occur.

II. LINEAR THEORY

A. OAM Plasma Waves

To aid in understanding of the work carried out in this study we briefly restate the formalism used for description of OAM plasma waves [8]. Firstly we consider a small amplitude plasma wave described by an electrostatic potential Φ and electron distribution function f related by the Poisson equation:

$$\nabla\Phi = \frac{e}{\epsilon_0}\delta n_e = \frac{e}{\epsilon_0}\int \mathrm{d}\mathbf{v}\delta f_e, \tag{1}$$

where the solutions to the paraxial equation in the limit $1/kw_{b,0} \ll 1$, are of the form:

$$\Phi(z,r,\theta,t) = \sum_{p,l} \phi_{p,l} F_{p,l} \exp(-i\omega t + ikz + il\theta + i\psi_{p,l} + iqX), \tag{2}$$

$$f(z,r,\theta,\mathbf{v},t) = \sum_{p,l} f_{p,l}(\mathbf{v}) F_{p,l} \exp(-i\omega t + ikz + il\theta + i\psi_{p,l} + iqX). \tag{3}$$

Here q is the term for front curvature, $X = r^2/w_b^2$ is the normalised radial coordinate, and $\psi_{p,l}$ is the Gouy phase. For this study we only consider a parallel propagating plasma wave (the beam waist w_b is considered constant) and so only consider the structure within the Rayleigh zone $|z| \ll z_R$, such that the contributions of q and $\psi_{p,l}$ are ignored. $F_{p,l}$ is the Laguerre-Gaussian function given by:

$$F_{p,l}(X) = C_{p,l} X^{|l|/2} L_p^{|l|}(X) e^{-X/2}, \tag{4}$$

$L_p^{|l|}$ is a generalised, or associated, Laguerre polynomial with radial mode integer $p \geq 0$ and azimuthal mode integer l, and $C_{p,l} = \sqrt{p!/(|l|+p)!}$ is a normalisation factor to ensure that solutions are orthonormal. However, as presented in Ref. [8] for the Vlasov equation, the solutions given in Eq. (2) are not plasma wave eigenmodes and so neighbouring modes are in fact coupled in higher orders of the paraxial parameter $1/kw_b$.

B. Electric Field

For simplicity we consider here a structure of a single mode p and use the electric potential given in Ref. [8] containing only one term characterised by the amplitude $\phi_{p,l}$:

$$\Phi(z, r, \theta) = \phi_{p,l} F_{p,l}(X) \cos(kz - \omega t + l\theta), \tag{5}$$

where the radial part is given by the function $F_{p,l}(r^2/w_b^2)$ (4). The electric field is found by taking the gradient of the potential:

$$E_z = E_0 F_{p,l}(X) \sin(kz - \omega t + l\theta), \tag{6}$$

$$E_\theta = \frac{lE_0}{kw_b} X^{-1/2} F_{p,l}(X) \sin(kz - \omega t + l\theta), \tag{7}$$

$$E_r = -2\frac{E_0}{kw_b} X^{1/2} F'_{p,l}(X) \cos(kz - \omega t + l\theta), \tag{8}$$

where $E_0 = k\phi_{p,l}$ is the amplitude of the axial electric field. The axial field dominates, the transverse fields are smaller by a factor $1/kw_b$. When looking at Eqs. (7) and (8) one can immediately observe from these two equations that there is a ratio of $E_\theta/Ez = l/kr$.
A previously published calculation [11] has been performed to find the momentum gain from the electron equation of motion in an electric field described by Eqs. (6), (7), and (8). This calculation is made assuming a small first order change, which would still be in the realm of a small deviation occurring per plasma oscillation. These calculations yield a ratio of $\Delta v_\theta/\Delta v_z = l/kr$, or considering the change in radial position as well $\Delta(rv_\theta)/\Delta v_z = l/k$. If we consider the change in orbital angular momentum, then $\Delta l_z/\Delta p_z = l/k$ where Δl_z is the change in specific orbital momentum about the axis z.

III. NUMERICAL SIMULATION SETUP

A. Plasma Wave Amplification

For this study the particle-in-cell (PIC) code OCEAN [12] is used. To create a stable plasma wave a similar initialization to that described in Refs. [8, 11] can be used to adiabatically drive a plasma wave for a small number of oscillations. An electric field is volumetrically imposed according to Eqs. (6), (7), and (8). Several simulations are run, each for a single mode, the first with a standard Gaussian profile, with $l = 0$ and $p = 0$,

the remaining three simulations with $p = 0$ and an $l = 1$, 2 and 4. The simulation box boundaries are reflecting on the transverse edges, to preserve any OAM particles may have gained, and periodic along the wave propagation axis in order that the wave can be excited. For these simulations a plasma is set up so that a cold phase velocity of $\omega_{pe}/k = 0.53\ c$ is chosen, with an initial temperature $T_e = 0.03\ m_e c^2$ such that $v_{th} = 0.173\ c$. Here, ω_{pe} is the plasma frequency and $v_{th} = \sqrt{T_e/m_e}$ is the electron thermal velocity. The resolution and temperature are set so that $\lambda_{De} = 1.208\ \Delta x$ and the time-step $\Delta t = 0.01318\ T_{pe}$, where $\lambda_{De} = v_{th}/\omega_{pe}$ is the plasma Debye length and $T_{pe} = 2\pi/\omega_{pe}$ is the plasma wave period. The grid resolution is observed to be sufficient to ensure energy conservation and other non-physical effects for at least 4000 δt. The plasma wave transverse width is $w_b = 0.95\ \lambda_{pe}$, where $\lambda_{pe} = 2\pi/k$ is the plasma wavelength, so that the paraxial parameter is $kw_b = 6$.
The waves are initially driven with the described electric field over 5 periods with a dimensionless amplitude $eE_0/m_e\omega_{pe}c = 0.08$ (e being the electron charge, m_e being electron mass, and E_0 being the amplitude of the electric field). The amplitude of the plasma waves reach only $eE_0/m_e\omega_{pe}c \sim 0.025$, due to a slight mismatching between the phase of the imposed electric field and the plasma response, and due to the damping of the wave occurring during the amplification process. Despite these losses the total energy of each plasma wave mode produced in this way vary less than $\sim 3\%$ from the mean of the total energy of all of the plasma waves.
The simulation parameters are chosen foremost with the aim of studying the wave-particle interaction in three dimensions (3D) and being achievable computationally whilst also not having a Landau damping rate so high that no plasma wave survives. With the second concern being having some Landau damping at velocities that are observable within the PIC code given the limited number of particles per cell achievable in 3D. The amplitude of the wave is also carefully chosen so that the resulting plasma wave is not close to the wave-breaking regime whilst still being visible above PIC noise.

B. Model for the Tail of Electron Distribution Function

When generating a distribution of electrons in a 3D PIC simulation a good resolution of higher energy regions of the distribution function, e.g. regions greater than a few standard deviations from the mean velocity, is necessary in our case. To achieve a reasonable resolution

for the diagnostics related to the distribution function, for a moderate temperature plasma ($v_{th} \ll c$), the velocity distribution function along the wave propagation axis is split into three parts: a truncated Gaussian distribution such that the distribution is cut off at $-v_s < |v_z| < v_s$ and is symmetrical about the mean velocity. Two tail distributions truncated such that $|v_z| > v_s$. For the main body distribution a Box-Mueller transform can be used to generate a Maxwellian distribution followed by a simple accept-reject method to make the cut-offs at the $\pm v_s$ edges of the distribution. For the last two parts the method described in chapter 9, by Devroye [13], for sampling a Gaussian tail distribution is efficient enough that it can be employed to generate the two tail distributions for a split value of $v_s = 2.5\ v_{th}$.
When tested using a plasma wave with $v_{ph} = c$, so that no damping will occur (as in Ref. [8]), the simulations with multiple electron species and single species produce identical results. However, the simulations with lower values of $v_{ph} \simeq 3\ v_{th}$, where Landau damping is expected to be stronger, with just a single species of electrons were seen to artificially suppress Landau damping. When testing the number of particles required in the extra species to initiate damping, a small number were added to each simulation run until the behaviour was seen not to change significantly from run to run. The electrons in each simulation are split into two species, with 100 particles per cell for the main-body distribution, and 20 particles per cell for both tail ($\pm v_s$) distributions.
For this study only a split along the wave propagation direction is considered, whilst it is possible to add extra particles in the transverse direction it is not necessary for observing Landau damping of a wave with a phase velocity such that $v_{ph} \gg v_{th}$.

IV. SIMULATION RESULTS

A. Non-Linear Landau Damping and Particle Trapping

Finding a regime where linear Landau damping is clearly observable in a 3D PIC environment, whilst still resolving relevant processes, is extremely challenging. However obtaining results for a relatively stable non-linear regime is achievable.
The conditions in the presented PIC simulations, along with the extra resolution provided by the additional particle species, give rise to non-linear Landau damping as the bounce frequency $\omega_b = \sqrt{eE_0k/m_e} \simeq 0.7\omega_{pe}$ is nly slightly smaller than the plasma frequency. The

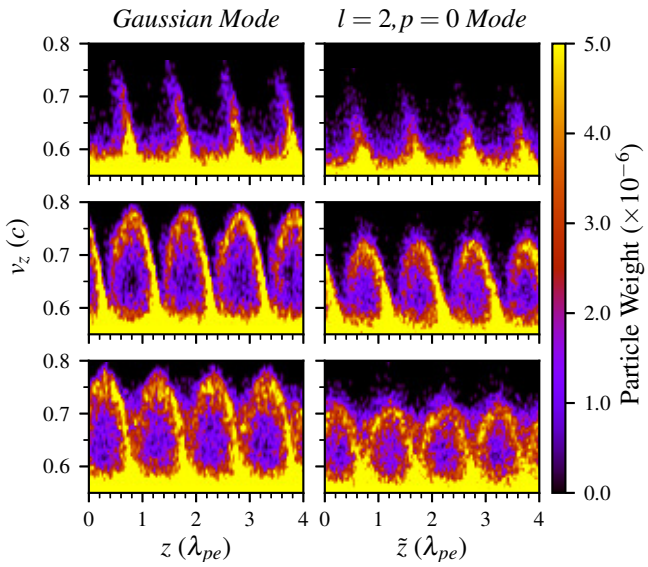

FIG. 1. Phase plots of p_z vs. z at different times for the Gaussian beam (left) and an $l = 2$ Laguerre-Gauss beam, the top row shows the simulations at $t = 3.1\ T_{pe}$, the second row $t = 6.3\ T_{pe}$ and the last row at $t = 9.4\ T_{pe}$ after the simulation has started. These plots are calculated by integrating over the whole range of r and θ. The Gaussian wave clearly shows rotation in the v_z, z space, this is not visible for the Laguerre-Gauss wave until the appropriate variable $(v_z, \tilde{z})$ is selected, where $\tilde{z} = z + l\theta/k$. As there is only a single mode with a single phase velocity in each simulation rotation is only visible in the positive v_z direction.

maximum amplitude achieved in the simulations is lower than the wave-breaking threshold [14] (i.e. $eE_0/m_e\omega_{pe} < v_{ph}$) and so wave-breaking is not observed. Another non-linearity to note is that the phase velocity (at the lowest condition for a Gaussian mode $\omega/k = 0.61\ c$ from the Bohm-Gross dispersion), while not strongly relativistic ($\gamma_{ph} = 1.26$) will lead to particles accelerating into relativistic regimes.

While these conditions present more difficulty in analysis and linking to linear theory, they do provide an interesting test to observe the transfer of OAM from an electrostatic plasma wave to higher energy particles. The rotation in phase space $(v_z, z)$for non-linear Landau damping is observable in Fig. 1, while the rotation is clearly observable in the Gaussian case as we can integrate over the whole transverse plane. In the higher LG modes this rotation is not visible at all, however if the phase space is 'untwisted' so that the axial coordinate is chosen as $\tilde{z} = z + l\theta/k$, the rotation is visible.

There are three distinct periods of time during the simulations which need to be considered.

The first period $t = 0 - 5\ T_{pe}$, is the time during which the plasma wave is amplified, with an increase in energy for both fields and particles. The second period $t = 3 - 4\ T_{pe}$ can be defined as a span of time, where quasi-linear Landau damping occurs (e.g. the wave dampens but at a slower rate than expected). Here the EM energy decreases, while the particle energy rises at the same rate. The final period $t > 8 - 9\ T_{pe}$, being the span of time where there is a dynamic exchange between the EM field energy and particle energy. As the damping rate is dependent on the gradient of the distribution function around the phase velocity, it can be expected that the distribution function is flattened out around the phase velocity starting during the second period and completing in the third period, this can be seen in Fig. 2.

A measurement of the reduction in the phase velocity can then be used to confirm the non-linear behaviour of Landau damping. It means a feedback on the wave phase velocity, which is reduced as the density of resonant particles decreases [15]. The phase velocity can be calculated by measuring the frequency of the wave by taking the Fourier transform over the time domain in the electric field measured at several points in space. When taking the longitudinal electric field E_z the measured value is $\omega/\omega_{pe} = 1.12 \pm 0.005$ (or $v_{ph} = 0.59\ c$ assuming constant k), which corresponds to a plasma frequency lower than the Bohm-Gross dispersion predicts, which is also lower than the dispersion calculated in Refs. [8, 11].

The average transverse transit time (v_{th}) of an electron accross the plasma wave is approximately 6 T_{pe}, while the approximate bounce period is $\sim 1.4\ T_{pe}$. This indicates, that while particles will remain trapped for some time, there is some irreversible loss of energy from the wave to trapped particles.

There are two caveats to note while analysing the numerical results obtained in the setup described above. The first caveat is that the theory developed in previous works [8, 11] supposes, for simplicity, a simple Maxwell-Boltzmann distribution, which given the magnitude of the phase velocity $v_{ph} \sim 0.6\ c$ may not be sufficient. Moreover, the Landau damping rate is a function of the gradient $\mathrm{d}f/\mathrm{d}v_z$ around the resonance region $v_z \sim v_{ph}$, which is slightly shallower in the Maxwell-Boltzmann distribution when compared to the more realistic (at least for higher T_e) Maxwell-Jüttner distribution.

The second caveat is that there are a finite number of particles in a periodic box. In this case the alteration of $\mathrm{d}f/\mathrm{d}v_z\big|_{v_{ph}}$ is much more significant as the gradient parallel to the wave propagation direction becomes flattened around phase velocity v_{ph} and so less momentum

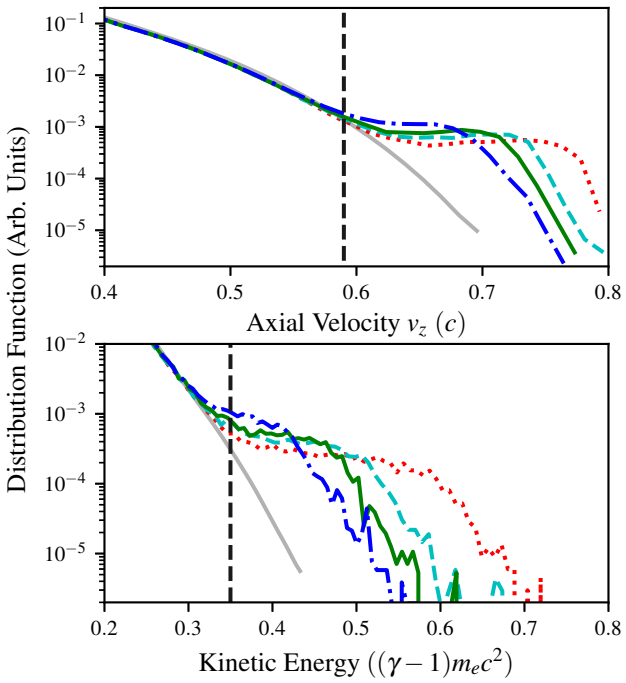

FIG. 2. Distribution of the velocity in the axial direction (top) and distribution of energy (bottom) at time $t = 5\ T_{pe}$ when oscillations after amplification has finished. The solid light grey line shows the initial conditions for the simulations. The red dotted line shows the distribution for the Gaussian wave simulation, the cyan line for the case of LG mode $l = 1$, the green dashed line for $l = 2$, and the solid blue line for $l = 4$. The vertical dashed black line in the top plot shows the magnitude of the measured phase velocity. The vertical dashed grey line in the bottom plot shows $E_k = 0.35\ m_ec^2$ relevant to Fig. 3.

is transferred from the electrostatic wave to the particles.

This may lead to a significant problem in comparing the measured phase velocity and damping rate that occurs in simulations like this to theoretical models, which assume fixed distribution functions. In this situation an appreciation of how momentum is transferred from the wave to the particles is possible and presented below.

B. Energy Distribution

It is important to note that in each simulation the same amount of energy is input via the amplification process, the same temperature is initially selected, and that the distribution function for particles with energies less than $\sim 0.35\ m_ec^2$ remain unchanged throughout the

length of the simulation (some 2000+ time steps). Despite the fact that the low energy particle behaviour is similar in each simulation the distribution of particles with energies higher than 0.35 $m_e c^2$ is quite different, both in the amount of energy each particle has (though the total energy is roughly constant) (see Fig. 2), and the distribution of that energy amongst the three components of velocity v_z, v_θ, and v_r (see Fig. 3).

In each of the simulations the gradient in the energy distribution around the high energy region (Fig. 2) starts to decrease almost immediately as the plasma-wave is amplified, after approximately $3-4$ periods after the amplification of the wave (approximately $8-9$ plasma periods, a steady state is reached where the energy transfer between the electric field and the particles becomes reversible and the rate of change of both becomes zero.

The distribution of energy in the high energy tail is significantly different depending on the mode chosen (see Fig. 2), with the Gaussian mode promoting fewer particles to higher energies (with a maximum $\sim 0.7\ m_e c^2$), whilst the modes with larger mode numbers have larger numbers of particles accelerated but to lower energies (with a maximum of $\sim 0.55\ m_e c^2$ in the case where $l = 4$). An interesting point to note is the reduction in the number of particles with very high energies at higher l, with $l = 4$ the distribution of energy of the accelerated particles looks closer to mono-energetic than those with lower mode numbers.

C. Momentum Distribution

The largest differences in resonant electron behaviour between the modes are apparent when looking at the distribution of momentum when resolved into axial p_z, azimuthal p_θ, and radial p_r components.

There does appear to be a structure to the assignment of angular and radial momentum when momentum is transferred from the electrostatic wave to the trapped particles. Figure 3 shows plots of v_z, v_θ, and v_r, from this it is clear to see that with increase l there is a decrease in $\langle v_z \rangle$ with a corresponding increase in $\langle v_\theta \rangle$. While $\langle v_r \rangle = 0$ the spread of the momentum increases slightly as a function of l, this change is noted to increase very slowly over time, unlike v_z and v_θ, it is possible that this is a ponderomotive effect (as the gradient of the radial electric field is dependent on l) that leads to particles leaving the plasma wave. This happens much later in time and so no conclusions are drawn about $\langle v_r \rangle$, or from later in the

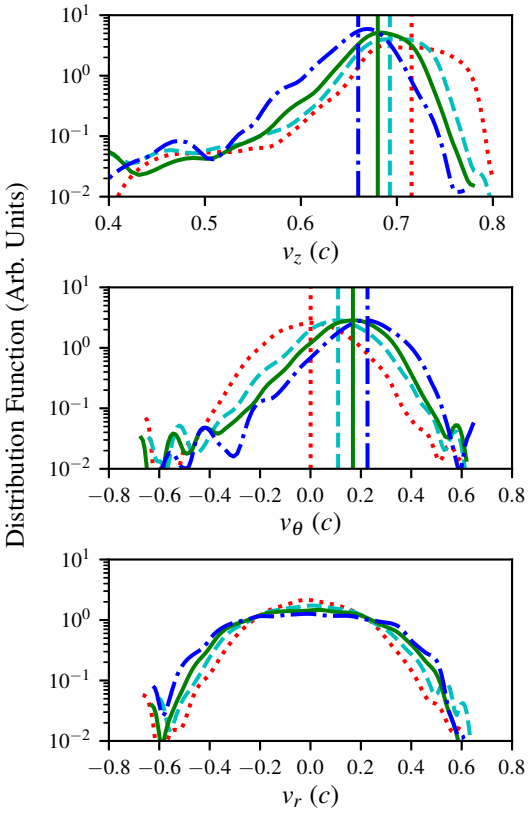

FIG. 3. Velocity distributions for particles with energies over $E_k > 0.35$ $m_e c^2$, split into the axial z direction (top), azimuthal θ direction (centre), and radial r direction (bottom). This plot uses the same line styles as in Fig. 2, where the red dotted line represents the $l = 0$, the cyan dashed line the $l = 1$, the green solid line $l = 2$, and the blue broken line $l = 4$. The vertical lines show the average velocity for each component except the bottom plot where $\langle v_r \rangle = 0$ for all simulations. The lines shown here are smoothed using a moving average over 5 bins.

simulation (past $\sim 20\ T_{pe}$).

The values for $\langle v_z \rangle$ and $\langle v_\theta \rangle$ can be seen in the second and third columns in Table I.

D. Angular Momentum Transfer

The average angular momentum would for a non-rotating plasma wave, be equal to zero. However as can be seen in the middle plot of Fig. 4 for plasma waves with non-zero azimuthal mode numbers the average is non-zero.

The distribution of particles as a function of $r v_\theta = l_z / \gamma m_e$ can be seen as the upper most

TABLE I. Mean Variables

Mode number l	$\langle v_z \rangle$ (c) $\pm \times 10^{-2}$	$\langle v_\theta \rangle$ (c) $\pm \times 10^{-2}$	$\langle r v_\theta \rangle_{v_z = v_{ph}}$ $\times 10^{-3} (c^2 \omega_{pe}^{-1})$
0	0.72	0.00	0.0 ± 1.0
1	0.69	0.11	0.4 ± 0.4
2	0.68	0.17	1.0 ± 0.5
4	0.66	0.23	3.0 ± 1.5

TABLE II. Average velocity and orbital momentum components as a function of azimuthal mode number l, the averages in the second and third columns are plotted in Fig. 3, the averages and errors are calculated from Gaussian function fits. The fourth column shows the average $\langle r v_\theta \rangle_{v_z = v_{ph}}$ with errors obtained from the fits taken in Fig. 4.

plot in Fig. 4. It is convenient to plot the negative and positive $r v_\theta$ overlaid so that the relative amount of $r v_\theta$ can be readily observed. For values of $r v_\theta$ in the range $0.55 \rightarrow 0.75$ a net positive orbital angular momentum can be seen, whilst above a certain threshold (~ 0.73 for $l = 4$, ~ 0.74 for $l = 2$, and ~ 0.75 for $l = 1$) orbital angular momentum is negative. The calculations performed in Ref. [11] suggest a linear relationship between the Δp_z and Δl_z as a function of the azimuthal mode number. Ideally to confirm this relationship a sum over the distribution function for the entire box would be calculated, however the level of noise in the main bulk of the plasma renders the errors on the sum too large to draw conclusions. Picking a specific velocity allows for a single point of comparison, for this a velocity equivalent to the measured phase velocity of the plasma waves ($v_{ph}/c = 0.59 \pm 0.01$) is taken $\langle r v_\theta \rangle_{v_z = v_{ph}}$. This is plotted in at Fig. 4, while a conclusion that the relationship between $r v_\theta$ and l is linear can be drawn, the errors on the actual readings are too large to confirm the linearity (see Table I), however there is a definite increase in $r v_\theta$ as a function of mode number.

V. CONCLUSIONS

There are several conclusive observations that can be made from this study. The first, and most significant, is that particles are observed to be trapped in OAM plasma waves.

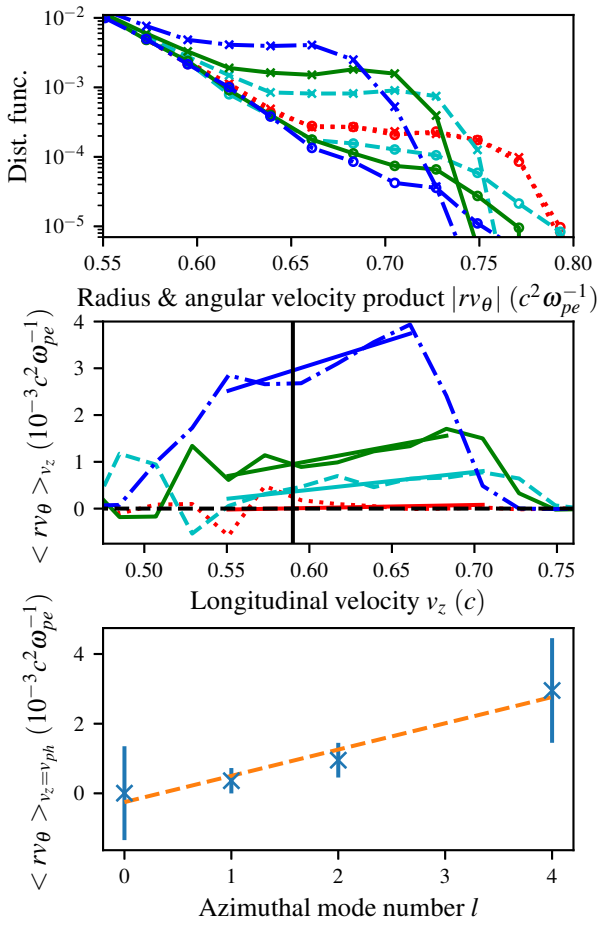

FIG. 4. Plots showing diagnostics of rv_θ (or $l_x/\gamma m_e$) at a time $t = 6.3\ T_{pe}$. The upper plot shows the distribution of the electron angular momentum rv_θ split into positive and negative parts ($\times$ for positive, $\circ$ for negative): the red dotted line corresponds to the Gaussian mode, the cyan dashed line to $l = 1$, the green solid line for $l = 2$, and the blue broken line shows the $l = 4$ case. The central plot shows $\langle rv_\theta \rangle$ as a function of v_z. The solid black vertical line is the phase velocity $v_{ph} = 0.59$, the straight solid lines show associated fits to each case. The bottom plot shows a single $\langle rv_\theta \rangle$ at a point $v_z = v_{ph}$ from the fits shown on the middle plot as a function of l with a linear best fit.

These trapped elecctrons are shown to be trapped in a phase space with the same twisted geometry as the OAM plasma waves themselves. Fig. 1 shows the same rotation in phase space for OAM plasma waves as is seen with planar waves when the space is transformed to take into account the rotation of the OAM.

The second conclusion worthy of note is that the energy distributions of electrons in damp-

ing Laguerre-Gaussian plasma waves are significantly changed as a function of azimuthal mode number. This leads to larger numbers of lower energy particles tending towards a mono-energetic bunching, see Fig. 2.

The third is that angular momentum is transferred from the plasma wave to the resonant electrons when Laguerre-Gaussian plasma waves are subject to Landau damping. In addition this transfer of OAM is proportional to the transfer of longitudinal momentum, see Fig. 3.

Lastly, it is observed, from results shown in Fig. 4, that the damping of a plasma wave with a higher azimuthal mode number leads to a larger net orbital angular momentum l_z in particles travelling close to v_{ph}. This implies the existence of a population of electrons, with a longitudinal velocity close to the phase velocity of the plasma wave, that are orbiting the same centre of rotation as the plasma wave.

ACKNOWLEDGMENTS

This work was granted access to HPC resources of TGCC under the allocation A0010506129 made by GENCI. We acknowledge PRACE for awarding us access to resource Joliot Curie-SKL based in France at TGCC Center. The authors acknowledge support from MEPhI Academic Excellence Project (Contract No. 02.a03.21.0005-27.08.2013). This research was partially supported by the Project LQ1606 with the financial support of the Ministry of Education, Youth and Sports as part of targeted support from the Czech National Programme of Sustainability II. This research was also supported by The National Science Foundation USA (PHY 1903098).

[1] L. Allen, M. W. Beijersbergen, R. J. C. Spreeuw, and J. P. Woerdman, "Orbital angular momentum of light and the transformation of Laguerre-Gaussian laser modes," *Phys. Rev. A*, vol. **45**, pp. 8185–8189, Jun. 1992.

[2] Q. Zhan, "Cylindrical vector beams: from mathematical concepts to applications," *Adv. Opt. Photonics*, vol. **1**, p. 1, Jan. 2009.

[3] J. Vieira and J. T. Mendonça, "Nonlinear Laser Driven Donut Wakefields for Positron and Electron Acceleration," *Phys. Rev. Lett.*, vol. **112**, p. 215001, May 2014.

[4] Z. Lécz, A. Andreev, and A. Seryi, "Plasma rotation with circularly polarized laser pulse," *Laser Part. Beams*, vol. **34**, pp. 31–42, Mar. 2016.

[5] J. Vieira, J. T. Mendonça, and F. Quéré, "Optical Control of the Topology of Laser-Plasma Accelerators," *Phys. Rev. Lett.*, vol. **121**, p. 054801, Jul. 2018.

[6] R. Nuter, P. Korneev, I. Thiele, and V. Tikhonchuk, "Plasma solenoid driven by a laser beam carrying an orbital angular momentum," *Phys. Rev. E*, vol. **98**, p. 033211, Sep. 2018.

[7] J. T. Mendonca, S. Ali, and B. Thidé, "Plasmons with orbital angular momentum," *Phys. Plasmas*, vol. **16**, p. 112103, Nov. 2009.

[8] D. R. Blackman, R. Nuter, P. Korneev, and V. T. Tikhonchuk, "Kinetic plasma waves carrying orbital angular momentum," *Phys. Rev. E*, vol. **100**, p. 013204, Jul. 2019.

[9] Y. Shi, J. Vieira, R. M. G. M. Trines, R. Bingham, B. F. Shen, and R. J. Kingham, "Magnetic Field Generation in Plasma Waves Driven by Copropagating Intense Twisted Lasers," *Phys. Rev. Lett.*, vol. **121**, no. 14, p. 145002, 2018.

[10] J. T. Mendonça, "Kinetic description of electron plasma waves with orbital angular momentum," *Phys. Plasmas*, vol. **19**, p. 112113, Nov. 2012.

[11] D. R. Blackman, R. Nuter, P. Korneev, and V. T. Tikhonchuk, "Twisted Kinetic Plasma Waves," *J. Russ. Laser Res.*, vol. **40**, pp. 419–428, Sep. 2019.

[12] R. Nuter and V. Tikhonchuk, "Prepulse suppression and optimization of backward Raman amplification with a chirped pump laser beam," *Phys. Rev. E*, vol. **87**, p. 043109, Apr. 2013.

[13] L. Devroye, *Non-Uniform Random Variate Generation*. New York, NY: Springer New York, 1986.

[14] W. Kruer, *The Physics of Laser Plasma Interactions*. Redwood, CA: Addison-Wesley - CRC Press, 1988.

[15] N. A. Yampolsky and N. J. Fisch, "Simplified model of nonlinear landau damping," *Phys. Plasmas*, vol. **16**, no. 7, 2009.